Total reflection and large Goos-Hänchen shift in a semi-Dirac system

Hongxiang Xiang[1] and Feng Zhai[1,2,*]
[1]*Department of Physics, Zhejiang Normal University, Jinhua 321004, China*
[2]*Zhejiang Institute of Photoelectronics and Zhejiang Institute for Advanced Light Source, Zhejiang Normal University, Jinhua 321004, China*

(Received 9 November 2023; revised 10 January 2024; accepted 11 January 2024; published 25 January 2024)

Carriers in two-dimensional semi-Dirac materials exhibit massless and massive dispersions along two perpendicular directions. Here, we investigate theoretically their properties of transmission and Goos-Hänchen (GH) shift under an electric barrier. It is found that isolated transmission zeros are allowed (prohibited) when the electric barrier aligns with the parabolic (linear) dispersion direction. Such transmission zeros require the coexistence of evanescent and propagating states in the outgoing region, whose number and position depend on the barrier width and height. Under a wide barrier, huge GH shift can be achieved at a transmission zero close to a reflection zero and at a small incident angle. The polarity of the GH shift depends on the sign of the incident angle and is controlled by the relative position between the barrier height and incident energy. The isolated transmission zeros and enhanced GH shift with tunable polarity could be helpful for potential electron-optics applications of semi-Dirac systems.

DOI: 10.1103/PhysRevB.109.035432

I. INTRODUCTION

The presence of massless Dirac fermions in graphene leads to many extraordinary transport properties [1]. When a proper uniaxial strain is applied on graphene lattice, the two nonequivalent Dirac points merge into a single semi-Dirac point [2–4]. Carriers with energy near the semi-Dirac point behave relativistically and Schrödinger-like in two orthogonal directions [5–7]. Such a highly anisotropic electron dispersion has also been predicted in various materials and models, which include a TiO_2-VO_2 superlattice [8,9], strained organic salt [10], phosphorene under pressure and doping [11–13], black phosphorus under pressure [14–16], square lattice with half a magnetic-flux quantum per unit cell [17], photonic crystals [18], $Bi_{1-x}Sb_x$ thin film [19], striped boron sheet [20], topological insulators under magnetic proximity [21,22], monolayer arsenene [23], and silicene oxide [24]. Based on two-dimensional (2D) nonsymmorphic symmetries, spin-orbit semi-Dirac fermions have been proposed in Ref. [25]. Recently, it was predicted that the interplay between altermagnetism and nonsymmorphic symmetries can generate semi-Dirac points [26]. Semi-Dirac dispersion has been observed experimentally in a few-layer black phosphorene under the deposition of potassium atoms [27], tunable ultracold atomic honeycomb optical lattice [28], and polariton honeycomb lattices [29].

The low-energy physics of semi-Dirac systems may exhibit unique features in comparison with conventional semimetals and Dirac materials. For a 2D semi-Dirac system in an external magnetic field B, the electronic energy levels scale approximately as $B^{3/2}$ [5] and the magneto-optical absorption spectrum has an anisotropic (isotropic) selection rule for the interband (intraband) transition [30]. For a semi-Dirac nanoribbon, a conventional quantization of the Hall conductivity was demonstrated numerically, which is highly distinct from a Dirac system [4]. It was shown theoretically that the Fano factor of 2D semi-Dirac systems along the linear dispersion direction converges to a universal value [31] $F \approx 0.179$, which transits between the sub-Poissonian ($F \approx 1/3$) and the Poissonian ($F \approx 1$) limit at the band inversion and the insulating phase [32]. The semi-Dirac dispersion of a 2D electron system can be identified from the power-law decay of local density of states near a line defect [33] with decay index $-5/4$. The charge-pseudospin coupling in semi-Dirac graphene can be utilized to control the valley and chirality transport [34]. In normal-superconducting junctions based on semi-Dirac materials, the crossover from retro to specular Andreev reflection was predicted to be orientation dependent [35]. The presence of parabolic dispersion in semi-Dirac systems can significantly prolong the decay of the Ruderman-Kittel-Kasuya-Yosida interaction and enhance the Dzyaloshinskii-Moriya interaction around the relativistic direction [36]. It seems that unusual properties of semi-Dirac systems show up only when the transport is along (or near) the linear-dispersion direction. The electron-optics properties, especially the shift of electron beams, in semi-Dirac systems have received less attention.

It is well known that a light beam reflected totally by an interface of two dielectric media undergoes a lateral displacement relative to its incident position. This phenomenon, named Goos-Hänchen (GH) shift [37], is continuously enriched in optics [38–40] and has been developed to electron systems [41–43] and spin waves [44]. The similarity between photons and massless electrons has inspired extensive studies on GH shift of electrons in Dirac materials. In

*fzhai@zjnu.cn

graphene-based p-n-p junctions, the GH effect arises from pseudospin-dependent scattering and results in an $8e^2/h$ conductance plateau. Valley-dependent GH shift can be obtained in graphene under a local strain [45–47] and in tilted Dirac systems (such as 8-*Pmmn* borophene) under an electric barrier [48,49]. By applying an inhomogeneous time-periodically driving field on graphene, an anomalous GH shift in the inelastic channel has been revealed, whose sign can be tuned by the polarization of the laser field [50]. For electrons on the surface of a topological insulator with a potential barrier, the hexagonal warping effect leads to two transmitted beams with different GH shifts [51]. At a normal-metal/superconductor interface, GH-like shift in Andreev and normal reflection can be made negative and strongly modify the dispersion for the confined waveguide modes [52]. In Weyl semimetals, the GH shift and Imbert-Fedorov shift at the reflection interface are, respectively, valley independent and valley related [53], which depend on surface potentials [54] and interface materials [55,56].

In this work, for the transport along the parabolic direction of a semi-Dirac system, we demonstrate a salient electron-optics feature, i.e., giant GH shift at some isolated transmission zeros. In the literature, transmission zeros have been reported to appear in stubbed electron waveguides [57–59] and atomic chains [60,61]. For an electron traversing a thick potential barrier along the parabolic dispersion direction, we find multiple isolated transmission zeros by examining the phase drop of the transmission coefficient. These transmission zeros require the coexistence of evanescent and propagating modes in the outgoing region, which are absent when the transport is along the linear-dispersion direction. The GH shift of reflected electron beams is strictly zero under normal incidence, but can be huge at some transmission zeros and at a quite small incident angle.

II. MODEL AND FORMALISM

We consider a 2D electron system in the (x, y) plane showing a semi-Dirac dispersion, which is modulated by an electrostatic barrier $U(\vec{r})$. The effective low-energy Hamiltonian around the semi-Dirac point reads [2,33,62]

$$\hat{H} = -i\hbar v\sigma_y\partial_x - \frac{\hbar^2}{2m}\sigma_x\partial_y^2 + U(\vec{r})\sigma_0, \tag{1}$$

where v is the Dirac quasiparticle velocity along the massless (x) direction, σ_x and σ_y are Pauli matrices, σ_0 is the 2×2 unit matrix, and m is the effective mass along the parabolic (y) direction. For notational convenience, hereafter we express all quantities in dimensionless units by means of the characteristic energy $E_0 = 2mv^2$ and length $l_0 = \hbar/(2mv)$. In tetralayered black phosphorus (TBP) under a proper interlayer bias [63], one has $v = 1.2\times 10^5$ m/s and $m = 0.92m_e$, where m_e is the free electron mass. Accordingly, the energy and length units are $E_0 = 0.15$ eV and $l_0 = 0.52$ nm.

We focus on the case that the transport is along the parabolic direction where $U(\vec{r}) = U(y)$ vanishes outside the region $0 < y < d$ [see the inset of Fig. 1(b)]. The momentum component $\hat{p}_x = -i\partial_x$ is thus conserved. For an electron with energy $E > 0$ and transverse momentum k_x incident from the left of the barrier, the wave function $\Psi(x, y)$ can be written as

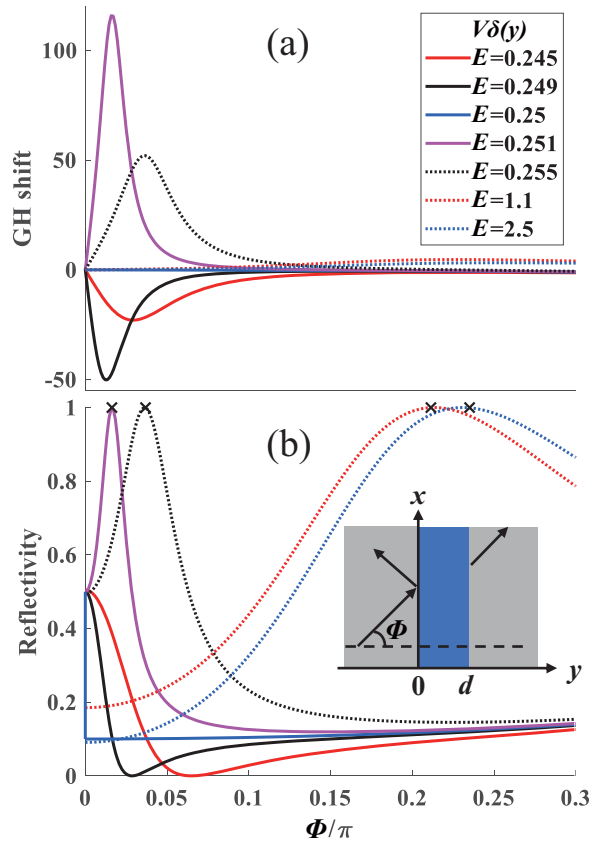

FIG. 1. Variation of (a) GH shift $s_{\rm GH}$ and (b) reflectivity $|r|^2$ with the incident angle Φ for the barrier $V\delta(y)$ (width $d \to 0$) and under different incident energies. The crosses mark the incident angles of total reflection at different energies. We set $V = 1$. The inset of (b) depicts the transport along the parabolic (y) direction of an electron with incident angle Φ, where the blue rectangular region represents the barrier with a width d. The energy and length units for the considered semi-Dirac system (TBP) are $E_0 = 0.15$ eV and $l_0 = 0.52$ nm.

$\Psi(x, y) = e^{ik_x x}\psi(y)$, where $\psi(y)$ satisfies $H_{k_x}\psi(y) = E\psi(y)$ with the reduced Hamiltonian

$$H_{k_x} = k_x\sigma_y - \sigma_x\partial_y^2 + U(y)\sigma_0. \tag{2}$$

In the left region $(y < 0)$ and right region $(y > d)$, one can write $\psi(y)$ as

$$\psi_{\rm L}(y) = (e^{ik_{\rm L}y} + re^{-ik_{\rm L}y})\begin{pmatrix}1\\ m_+\end{pmatrix} + r'e^{k_{\rm L}y}\begin{pmatrix}1\\ m_-\end{pmatrix},$$
$$\psi_{\rm R}(y) = te^{ik_{\rm L}(y-d)}\begin{pmatrix}1\\ m_+\end{pmatrix} + t'e^{-k_{\rm L}(y-d)}\begin{pmatrix}1\\ m_-\end{pmatrix}. \tag{3}$$

Here, r and t are the reflection and transmission coefficient, r' and t' are the coefficients of the decaying wave in the left and right region, and

$$k_{\rm L} = \left(E^2 - k_x^2\right)^{1/4} > 0, \quad m_\pm = \left(ik_x \pm k_{\rm L}^2\right)/E. \tag{4}$$

For the incident wave $\Psi(\vec{r}) = e^{ik_x x + ik_{\rm L}y}\psi_{\rm in}$ with $\psi_{\rm in}(k_x) = (1, m_+)^T$, the group velocity along the x and y directions is

given by

$$v_x = \frac{\psi_{\rm in}^\dagger \sigma_y \psi_{\rm in}}{\psi_{\rm in}^\dagger \psi_{\rm in}} = k_x/E,$$
$$v_y = \frac{\psi_{\rm in}^\dagger (2k_{\rm L}\sigma_x)\psi_{\rm in}}{\psi_{\rm in}^\dagger \psi_{\rm in}} = 2k_{\rm L}^3/E.$$

Then the incident angle Φ satisfies

$$\tan\Phi = \frac{v_x}{v_y} = \frac{k_x}{2k_{\rm L}^3}. \tag{5}$$

It can be seen from Eq. (3) that the propagating mode and evanescent mode coexist in the outgoing region. This fact allows the appearance of transmission zero ($t = 0$) or total reflection in the presence of an outgoing mode. This kind of transmission zeros (assisted by evanescent states) is forbidden when the transport is along the linear-dispersion direction. Actually, in the case $U(\vec{r}) = U(x)$, when the the outgoing mode exists but has a zero amplitude, the corresponding wave function is zero in the outgoing region. The continuity conditions and the related differential equation require that the wave function should vanish in all regions. However, the wave function is nonzero in the ingoing region. Such an argument can be applied to a Schrödinger particle with a parabolic dispersion or a Dirac particle with a linear dispersion traversing an electrostatic barrier.

For a wave packet consisting of incident electrons with the same energy E and transverse momenta centered at k_x, the GH shift $s_{\rm GH}$ of the reflected beam is defined as the difference between the lateral position (at the interface $x = 0$) of the reflected and incident electron beam [64,65]. The general expression is given by [48]

$$s_{\rm GH} = \frac{-{\rm Im}\left[\psi_r^\dagger(k_x)\frac{\partial\psi_r(k_x)}{\partial k_x}\right]}{\psi_r^\dagger(k_x)\psi_r(k_x)} + \frac{{\rm Im}\left[\psi_{\rm in}^\dagger(k_x)\frac{\partial\psi_{\rm in}(k_x)}{\partial k_x}\right]}{\psi_{\rm in}^\dagger(k_x)\psi_{\rm in}(k_x)}. \tag{6}$$

Here, $\psi_r(k_x) = r(1, m_-)^T$. After some algebra, we yield

$$s_{\rm GH} = -\frac{d[\arg(r)]}{dk_x}. \tag{7}$$

Note that the reflection coefficient r and GH shift $s_{\rm GH}$ depend on both the incident energy E and transverse momentum k_x (incident angle Φ). Since the operation σ_x changes H_{k_x} into H_{-k_x}, the reflection coefficient $r = r(E, k_x)$ satisfies

$$r(E, -k_x) = r(E, k_x). \tag{8}$$

Such a symmetry relation together with Eq. (7) and Eq. (5) leads to

$$s_{\rm GH}(E, -k_x) = -s_{\rm GH}(E, k_x),$$
$$s_{\rm GH}(E, -\Phi) = -s_{\rm GH}(E, \Phi). \tag{9}$$

The GH shift $s_{\rm GH}$ is thus an odd function of the incident angle Φ, which is exactly zero at normal incidence ($\Phi = 0$). It is sufficient to consider the situation $\Phi \geqslant 0$.

III. TOTAL REFLECTION AND GH SHIFT UNDER A δ BARRIER

Under a δ barrier $U(y) = V\delta(y)$ with width $d = 0$ and intensity V, from Eq. (2) one can obtain the matching conditions for the wave function $\psi_{\rm L}$ and $\psi_{\rm R}$ in Eq. (3),

$$\psi_{\rm L}(y)|_{y=0^-} = \psi_{\rm R}(y)|_{y=0^+},$$
$$\sigma_x[\partial_y\psi_{\rm R}(y)|_{y=0^+} - \partial_y\psi_{\rm L}(y)|_{y=0^-}] = V\psi_{\rm L}(y)|_{y=0}. \tag{10}$$

Based on Eq. (10), one can work out the four unknowns r, t, r', and t'. The reflection coefficient satisfies [33]

$$r^{-1} = -1 + 2i\frac{VE - 2\left(E^2 - k_x^2\right)^{3/4}}{V^2\left(E^2 - k_x^2\right)^{1/4} - 2VE}, \tag{11}$$

when $(E^2 - k_x^2)^{1/4} \neq 2E/V$. At normal incidence $k_x = 0$, one gets

$$r(E, k_x = 0) = \frac{1}{-1 + 2i\sqrt{E}/V}. \tag{12}$$

From Eq. (11), one can find the condition for the total reflection $|r| = 1$ (or transmission zero $t = 0$),

$$k_{\rm L} = \left(E^2 - k_x^2\right)^{1/4} = (EV/2)^{1/3} \neq 2E/V. \tag{13}$$

Since $k_{\rm L} \leqslant E^{1/2}$, Eq. (13) indicates that the total reflection happens only at $E > V^2/4$. Further, the reflection coefficient at the critical energy $E_{\rm c} = V^2/4$ changes discontinuously with k_x,

$$\lim_{k_x\to 0} r(E = V^2/4, k_x) = \frac{1}{-1 - 3i},$$
$$r(E = V^2/4, k_x = 0) = \frac{1}{-1 + i}. \tag{14}$$

This kind of discontinuity in the scattering coefficient has been rarely reported. From Eq. (12), one can see that the reflection coefficient at $k_x = 0$ changes continuously with the incident energy E.

By substituting Eq. (11) into Eq. (7), we yield the analytical expression of the GH shift,

$$s_{\rm GH} = \frac{12VEk_x/k_{\rm L} - 4V^2k_x - V^3Ek_x/k_{\rm L}^3}{(V^2k_{\rm L} - 2VE)^2 + 4\left(VE - 2k_{\rm L}^3\right)^2}. \tag{15}$$

Due to the presence of discontinuity (14), how to define the GH shift $s_{\rm GH}$ at $E = V^2/4$ and $k_x = 0$ deserves further discussion, which is beyond the scope of this work.

In Fig. 1, we plot the GH shift $s_{\rm GH}$ of the reflected electron beam and reflectivity $|r|^2$ as functions of the incident angle Φ. The intensity of the δ barrier is fixed at $V = 1$ so that the critical energy is $E_{\rm c} = 0.25$. At $E = E_{\rm c}$, the GH shift is small [$|s_{\rm GH}| < 1.01\ l_0$ (0.5252 nm)] in the considered region $0 < \Phi \leqslant 0.3\pi$. As shown in Fig. 1(b), the reflectivity at $E = E_{\rm c}$ increases slowly with Φ, where the discontinuity at $k_x = 0$ agrees with Eq. (14). When E is slightly lower than $E_{\rm c}$ such as $E = 0.249$, the GH shift decreases from zero to a negative minimum $<-50\ l_0$ (-26 nm) as Φ increases from 0 to 0.0135π [see Fig. 1(a)]. The reflectivity at $E = 0.249$ decreases from 0.5 to 0 and then increases to a value 0.137. Total reflection is not observed for $E = E_{\rm c} - 0.005$, $E = E_{\rm c} - 0.001$, and $E = E_{\rm c}$. For $E > E_{\rm c}$, total reflection appears as a reflection peak [marked as the leftmost cross in Fig. 1(b)]. The GH shift for $E > E_{\rm c}$ exhibits a positive maximum at the incident angle where the total reflection happens. For E approaching $E_{\rm c}$ from above, one can see a sharp peak of

$s_{\rm GH}$ with value exceeding 100 l_0 (52 nm). Accordingly, the GH shift can be remarkable in amplitude for E near $E_{\rm c}$, and change sign as E crosses $E_{\rm c}$. By comparing the GH shift under $|E - E_{\rm c}| = 0, 0.001$, and 0.005, one can see that the maximum absolute GH shift (max $|s_{\rm GH}|$) increases as the incident energy approaches the critical energy ($E \to E_{\rm c}$). Accordingly, one can obtain a large GH shift by setting the incident energy very close to the critical energy.

IV. TOTAL REFLECTION UNDER A SQUARE BARRIER

To further confirm the presence of total reflection assisted by evanescent waves, we consider the example of a square barrier $U(y) = V\Theta(y)\Theta(d-y)$ with barrier height V and barrier width d. Here, $\Theta(y)$ is the Heaviside step function. The wave function in the barrier region $0 < y < d$ can be written as

$$\psi_{\rm M}(y) = (ae^{ik_{\rm M}y} + be^{-ik_{\rm M}y})\begin{pmatrix}1\\ n_+\end{pmatrix} + (ce^{-k_{\rm M}y} + de^{k_{\rm M}y})\begin{pmatrix}1\\ n_-\end{pmatrix}, \tag{16}$$

where $k_{\rm M} = [(E-V)^2 - k_x^2]^{1/4}$, $n_\pm = (ik_x \pm k_{\rm M}^2)/(E-V)$. The eight unknown coefficients r, r', a, b, c, d, t, and t' in Eqs. (3) and (16) can be determined from the matching conditions of the wave functions at the boundary $y = 0$ and $y = d$, i.e.,

$$\begin{aligned}\psi_{\rm L}(0) &= \psi_{\rm M}(0),\\ \psi_{\rm M}(d) &= \psi_{\rm R}(d),\\ \frac{d\psi_{\rm L}(y)}{dy}|_{y=0} &= \frac{d\psi_{\rm M}(y)}{dy}|_{y=0},\\ \frac{d\psi_{\rm M}(y)}{dy}|_{y=d} &= \frac{d\psi_{\rm R}(y)}{dy}|_{y=d}.\end{aligned} \tag{17}$$

One can straightforwardly obtain an analytical expression for the reflection coefficient r, which is, however, rather lengthy. Instead, we calculate the scattering coefficient r and t by means of the numerically stable scattering matrix method [66–68].

At a first-order transmission zero $E_{t=0}$, there is a phase discontinuity [59,60], i.e., $\Delta \arg[t(E)] = \arg[t(E^+)] - \arg[t(E^-)]$ equals $\pm\pi$ at $E = E_{t=0}$. For a given transverse momentum $k_x \geqslant 0$, the first-order transmission zeros are determined as follows. First, we sweep the incident energy E to find the narrow energy intervals $[E_{1i}, E_{2i}]$ embracing a first-order transmission zero E_{0i}, where $|\arg[t(E_{2i})] - \arg[t(E_{1i})]| > 0.25\pi$. Here the index i is used to identify different transmission zeros. Then the bisection method is used to find the value of $E_{0i} = (E_{1i} + E_{2i})/2$ with tolerance $|E_{2i} - E_{1i}| < 10^{-14}$, $|t(E_{0i})| < 10^{-14}$, and $\min_{s=\pm1} |\arg[t(E_{2i})] - \arg[t(E_{1i})] + s\pi| < 10^{-7}\pi$. Based on the analytical expression of t, we can calculate the complex integral $\oint_{|E-E_{0i}|=\epsilon} t^{-1}(E)\frac{dt(E)}{dE}dE$ to confirm the presence of transmission zero near E_{0i} with tolerance ϵ.

In Fig. 2, we plot the energy of first-order transmission zeros as a function of the transverse momentum k_x. The barrier height is fixed at $V = 1$. The results under several values of barrier width d are compared to that under a δ barrier [Eq. (13)]. For a given $k_x > 0$, one can find only one

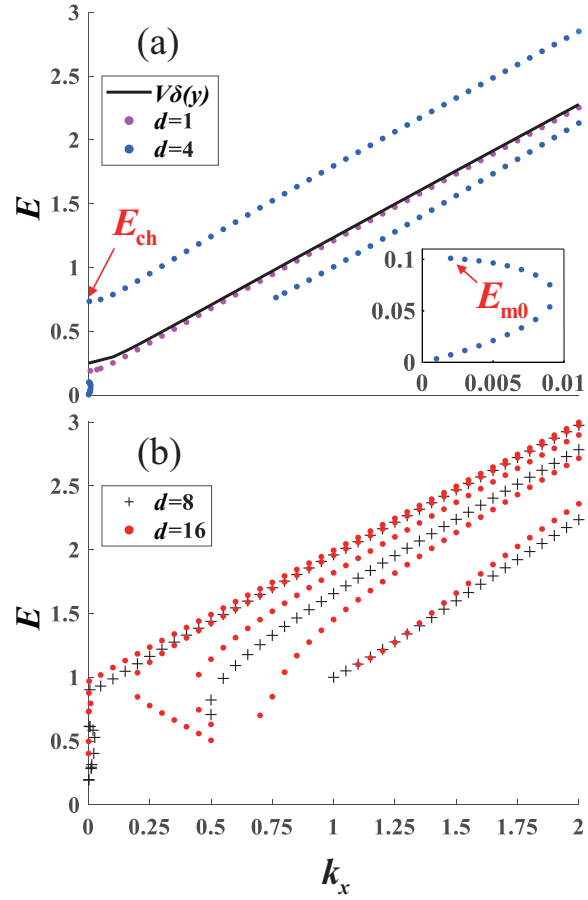

FIG. 2. Energy of transmission zeros plotted as a function of the transverse momentum k_x for rectangular barriers with the same height $V = 1$ but different widths. (a) $d = 1$ and 4; (b) $d = 8$ and 16. The result for the δ barrier [Eq. (13)] is plotted in (a) for comparison. The inset of (a) plots the transmission zeros near normal incidence under $d = 4$, which has maximum energy $E_{\rm m0} = 0.101$. $E_{\rm ch}$ is the onset energy of the highest branch of transmission zeros, which equals 0.735 in the case $d = 4$. The energy and length units for the considered TBP are $E_0 = 0.15$ eV and $l_0 = 0.52$ nm.

transmission zero for the δ barrier and the narrow square barrier with width $d = 1$. As shown in Fig. 2(a), the curves for the two cases almost coincide and are approximately linear for $k_x > 0.1$. For the width $d = 1$, the critical energy corresponding to the onset of transmission zero is slightly lower than that for the δ barrier. As the barrier width increases, several transmission zeros coexist at large transverse momentums. In the case $d = 4$, one can find two transmission zeros at $k_x \geqslant 0.765$. In the case $d = 8$ [Fig. 2(b)], the number of transmission zero is, respectively, 1, 2, and 3 for $0.03 \leqslant k_x \leqslant 0.496$, $0.536 \leqslant k_x \leqslant 0.96$, and $0.961 \leqslant k_x$. In the case $d = 16$, five transmission zeros coexist at $k_x \geqslant 1.1$. The highest energy of transmission zeros shows a nearly linear variation with k_x and a minor dependence on the width d. The onset energy $E_{\rm ch}$ of the highest branch of transmission zeros for the wide barrier is noticeably higher than that for the δ barrier. In the case of wide barriers $d \geqslant 4$, there are additional transmission zeros with k_x near zero and $E < E_{\rm ch}$ [see, for example, the inset of Fig. 2(a)].

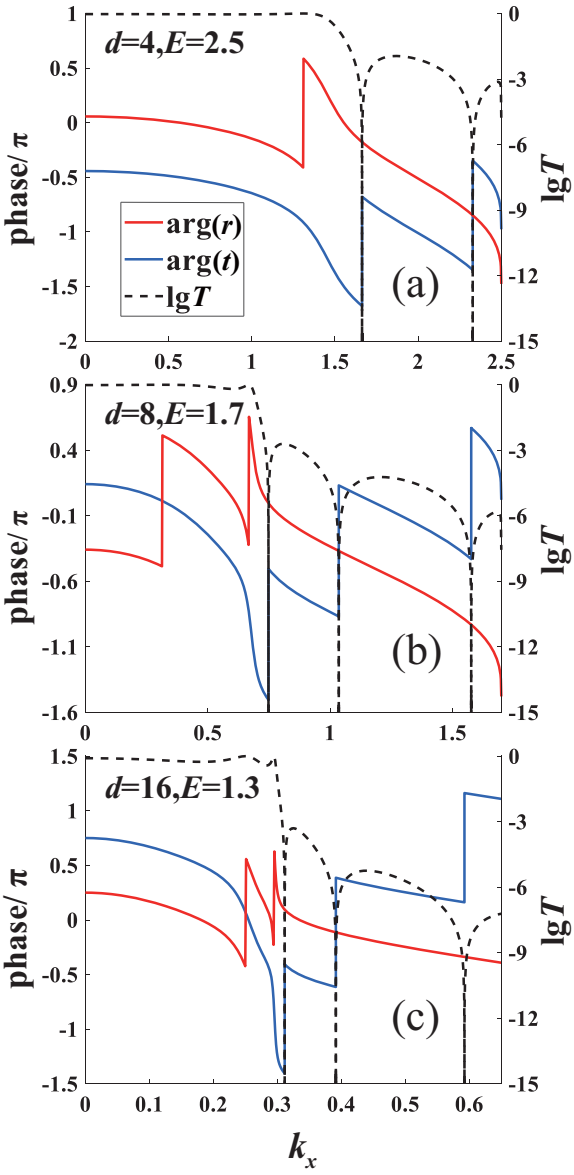

FIG. 3. Variation of scattering phase [arg(r) and arg(t)] and the decimal logarithm of the transmission (lg T) with transverse momentum k_x for different barrier widths and incident energies. (a) $d = 4$ and $E = 2.5$; (b) $d = 8$ and $E = 1.7$; (c) $d = 16$ and $E = 1.3$. We set $V = 1$. The energy and length units for the considered TBP are $E_0 = 0.15$ eV and $l_0 = 0.52$ nm.

For a given incident energy E, one can also find many transmission zeros with different transverse momenta, as shown in Fig. 3. Here the scattering phase arg(r) (red lines) and arg(t) (blue lines) together with the transmission $T = |t|^2$ are plotted as functions of the transverse momentum k_x. Under three barrier widths ($d = 4$, 8, and 16), the transmission phase arg(t) has a jump of π near each transmission zero (where $T < 10^{-15}$). The reflection phase arg(r) changes drastically near a perfect transmission. The jump of π for the reflection phase arg(r) at the first-order reflection zeros arises from the analytical properties [60] of the function $r(k_x)$ or $r(E)$. Under $d = 4$, there are two transmission zeros at a high energy $E = 2.5$, which are away from the discontinuity point of arg(r). Under $d = 8$ and at $E = 1.7$, one can observe three transmission zeros. The first transmission zero is close to the last discontinuity point of arg(r). Similar features are seen under $d = 16$, but at a smaller energy $E = 1.3$. From Eq. (7), one can expect a large GH shift near the first transmission zero.

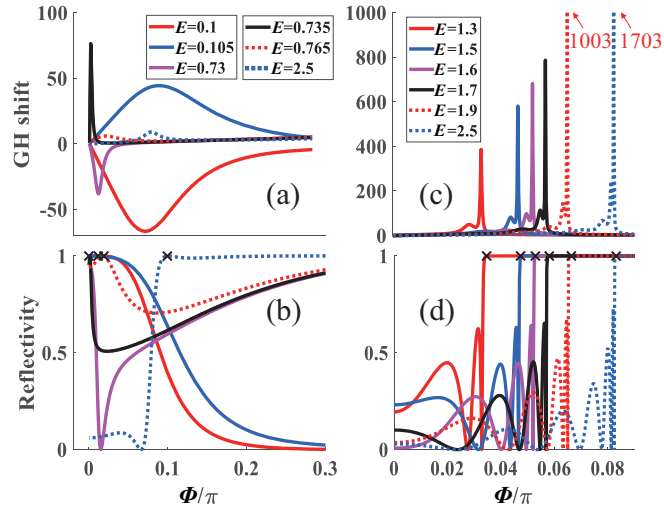

FIG. 4. Variation of the GH shift (upper panels) and reflectivity (lower panels) with the incident angle Φ under several values of the barrier width d and incident energy E. (a) and (b) $d = 4$; (c) and (d) $d = 16$. The barrier height is fixed at $V = 1$. In (c), the GH shifts beyond the vertical axis are marked with their maximum (numbers in red). The crosses in the lower panels mark the incident angles of total reflection at different energies. For the considered TBP, the energy and length units are $E_0 = 0.15$ eV and $l_0 = 0.52$ nm.

V. GH SHIFT UNDER A SQUARE BARRIER

For square barriers with different width d and the same height $V = 1$, we plot in Fig. 4 the GH shift $s_{\rm GH}$ of the electron reflected beam and reflectivity $|r|^2$ as functions of the incident angle Φ. The incident energy E is chosen to be either near (or above) the onset energy $E_{\rm ch}$ of the highest branch of transmission zeros, or close to the maximum energy $E_{\rm m0}$ ($< E_{\rm ch}$) of transmission zeros with small incident angles.

Under the width $d = 4$ [Fig. 4(a)], the GH shift shows a similar angular and energy dependence as that for the δ barrier. At a low energy $E = 0.1$, $s_{\rm GH}$ is negative and can be lower than $-65\ l_0$ (-34 nm). At $E = 0.105$, $s_{\rm GH}$ is positive and exceeds 44 l_0 (23 nm). Here the interval [0.1,0.105] contains $E_{\rm m0} = 0.101$ [see the inset of Fig. 2(a)]. The peak and trough of the GH shift are broad for E near $E_{\rm m0}$. For E near $E_{\rm ch}$, $s_{\rm GH}$ changes quickly with E and Φ. At an energy ($E = 0.735$) approaching $E_{\rm ch}$ from above, a sharp peak of $s_{\rm GH}$ [with height $>75\ l_0$ (39 nm)] appears in a narrow region of incident angle $0 < \Phi < 0.002\pi$. As $E > E_{\rm ch}$ is away from $E_{\rm ch}$ (such as $E = 0.765$), this peak of $s_{\rm GH}$ moves to the right and becomes weak. At $E = 0.73 < E_{\rm ch}$, a narrow trough of $s_{\rm GH}$ [with value $<-38\ l_0$ (-20 nm)] is observed. By inspecting the reflectivity shown in Fig. 4(b), one can see a steep slope of the reflectivity at the extremum of the GH shift. At E around $E_{\rm ch}$ ($E_{\rm m0}$), the reflectivity decays quickly (slowly) near $\Phi = 0$,

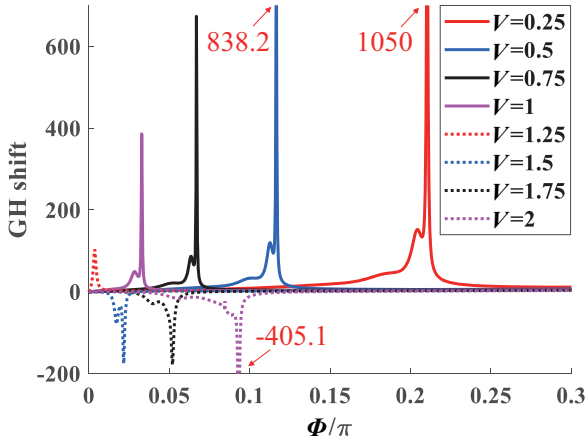

FIG. 5. Variation of the GH shift with the incident angle under different values of barrier height V. We set $d = 16$ and $E = 1.3$. The maximum or minimum of the GH shift beyond the range of the vertical axis is marked with their values (numbers in red). For the considered TBP, the energy and length units are $E_0 = 0.15$ eV and $l_0 = 0.52$ nm.

corresponding to a narrow (broad) peak of $s_{\rm GH}$. As E changes from 0.73 to 0.765, the minimum of reflectivity increases from 0 to 0.705. We note the reappearance of reflection zero at high incident energies (such as $E = 2.5$), which is followed by a relatively low peak of $s_{\rm GH}$ and a transmission zero.

The GH shift under a large barrier width $d = 16$ is plotted in Fig. 4(c) for $E > E_{\rm ch}$. There exist sharp peaks of $s_{\rm GH}$ in the narrow angular interval $0 < \Phi < 0.09\pi$. As the incident energy E increases, both the values and angular positions of these peaks move up. The GH shift can exceed 1703 l_0 (886 nm) at $E = 2.5$. As shown in Fig. 4(d), such a giant enhancement of GH shift happens near a transmission zero which is very close to a reflection zero. Consequently, at this transmission zero, a remarkable GH shift can be obtained. In addition, we can see several reflectivity maxima before the transmission zero. The GH shift at these reflectivity peaks, although comparable to the maximum of $s_{\rm GH}$ under $d = 4$, is much lower than that at the transmission zero.

It is desirable that the GH shift of the system with semi-Dirac points can be tuned electrically, i.e., changes remarkably with the barrier height V. For a typical incident energy $E = 1.3$ and barrier width $d = 16$, such a tunability is shown in Fig. 5. Under $0.25 \leqslant V < E$, the GH shift is positive and can exceed 1050 l_0 (546 nm), a value 65 times larger than the barrier width. The maximum of GH shift decreases with the barrier height. For $V > E$, the GH shift is negative and can be lower than -405 l_0 (-211 nm). This indicates that both the amplitude and polarity of $s_{\rm GH}$ can be tuned by the barrier height. As V increases from 0.25 to 2, the maximum of $|s_{\rm GH}|$ moves first towards the small incident angle and then turns back. In addition, the GH shift under $-2 \leqslant V \leqslant -0.25$ (not shown here) slightly changes with V and has a small amplitude [$|s_{\rm GH}| < 10$ l_0 (5.2 nm) in the range $0 \leqslant \Phi \leqslant 0.3\pi$].

VI. CONCLUSIONS

In summary, we have studied the presence of transmission zeros and GH shift of reflected electron beams for a 2D system with semi-Dirac points when the electric barrier aligns with the parabolic dispersion direction. The coexistence of evanescent and propagating states in the outgoing region allows the appearance of isolated transmission zeros. Such transmission zeros are absent when the electric barrier is along the linear-dispersion direction. The number and position of evanescent-state-assisted transmission zeros depend on the barrier width and height. When the incident energy is near the onset of the highest branch of transmission zeros, one can obtain both positive and negative GH shift with large amplitude at positive incident angles. Under a wide barrier, the above-barrier transmission zeros are very close to some reflection zeros. Accordingly, the GH shift at these transmission zeros is huge. In addition, the amplitude (polarity) of the GH shift depends on the distance (relative position) between the barrier height and incident energy. As demonstrated in the Appendix, the presence of transmission zeros and large GH shift are also sensitive to the angle between the transport direction and the parabolic dispersion direction. These findings could enrich the potential applications of the special dispersion relation of the semi-Dirac systems and provide a different approach to enhance the GH shift of reflected electron beams.

ACKNOWLEDGMENT

This work was supported by the National Natural Science Foundation of China (Grant No. 12274370).

APPENDIX: TRANSPORT ALONG OTHER DIRECTIONS

When the width direction ζ (length direction η) of the electric barrier is in an angle α to the x axis (y axis), i.e., $U(\vec{r}) = V\Theta(\zeta)\Theta(d-\zeta)$, the momentum operators $\hat{p}_x$ and $\hat{p}_y$ in Eq. (1) can be written as $\hat{p}_x = \hat{p}_\zeta \cos\alpha - \hat{p}_\eta \sin\alpha$ and $\hat{p}_y = \hat{p}_\eta \cos\alpha + \hat{p}_\zeta \sin\alpha$. Such a general case is depicted in the inset of Fig. 6. For the transport along the linear-dispersion direction ($\alpha = 0°$), the transmission zeros are absent, as argued in Sec. II. We thus focus on the case that α is close to 90°.

For an electron with a given energy E and conserved transverse momentum $p_\eta = q$, the wave function of the incident state has the form $\Psi(\vec{r}) = e^{iq\eta + ip\zeta}\psi_{\rm in}(q)$. The longitudinal momentum p satisfies

$$(p\cos\alpha - q\sin\alpha)^2 + (p\sin\alpha + q\cos\alpha)^4 = E^2. \qquad \text{(A1)}$$

Here the longitudinal velocity $v_\zeta = (\partial E/\partial p)|_q$ is positive. The presence of a real root p in Eq. (A1) requires $|q| \leqslant \sqrt{E^2 + |E|}$. From Eq. (A1), we can further obtain the transverse velocity $v_\eta = (\partial E/\partial q)|_p$ and the incident angle $\Phi = \arctan(v_\eta/v_\zeta)$. For such an incident state, the reflection and transmission coefficients (r and t) can be obtained by the scattering matrix method [66–68]. The GH shift is calculated from the formula in Ref. [48]. Note that at $\alpha = 90°$, the $+\eta$ axis is opposite to the $+x$ axis so that the angle Φ defined here is actually the opposite of that in Eq. (5).

In Fig. 6, the GH shift $s_{\rm GH}$ of the reflected electron beam is plotted as a function of the incident angle Φ under the barrier orientation $\alpha = 89°$ and 83°. We take the incident energy $E = 0.62$, barrier width $d = 8$, and barrier height $V = 1$. Now the GH shift is not antisymmetric on $\Phi = 0$ and $s_{\rm GH}(\Phi = 0) \neq 0$.

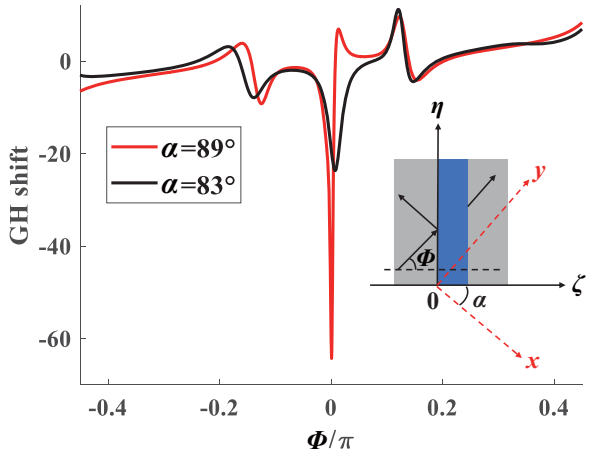

FIG. 6. Variation of the GH shift with the incident angle Φ under the barrier orientation $\alpha = 89^\circ$ and 83°. We set $E = 0.62$, $d = 8$, and $V = 1$. The inset depicts the transport along the ζ direction of an electron with incident angle Φ, where the ζ axis has an angle α relative to the x axis. The blue rectangular region represents the electric barrier. For the considered TBP, the energy and length units are $E_0 = 0.15$ eV and $l_0 = 0.52$ nm.

This observation is in contrast to the case of $\alpha = 90^\circ$ [see Eq. (9)]. At $\alpha = 89^\circ$, $s_{\rm GH}$ exhibits a narrow trough at $\Phi = 0.000\,874\pi$ [with value <-60 l_0 (-31 nm)]. At $\alpha = 83^\circ$, the GH shift reaches its extreme value -23 l_0 (-12 nm) at $\Phi = 0.007\,42\pi$.

The narrow trough of $s_{\rm GH}$ shown in Fig. 6 is related to the transmission zeros. In Fig. 7, we plot the scattering phase [arg(r) and arg(t)] and the transmission $T = |t|^2$ as functions of the transverse momentum q. The parameters are the same as in Fig. 6. Under $\alpha = 89^\circ$ [Fig. 7(a)], one can identify a transmission zero $q = 0$ from the phase jump π of t and the transmission minimum. Since arg(r) changes gradually near $q = 0$, the GH shift at this transmission zero is much smaller

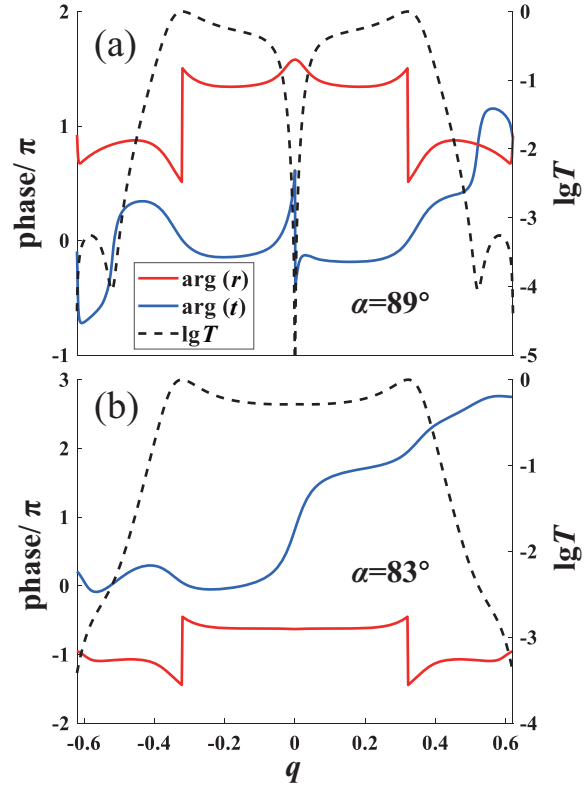

FIG. 7. Variation of scattering phase [arg(r) and arg(t)] and the decimal logarithm of the transmission (lg T) with transverse momentum q for different transport directions. (a) $\alpha = 89^\circ$ and (b) $\alpha = 83^\circ$. The parameters are the same as in Fig. 6.

than those in Fig. 4. Under $\alpha = 83^\circ$ [Fig. 7(b)], arg(t) changes continuously and $T > 10^{-4}$ in the considered interval of q. The transmission zero is absent. It is worth mentioning that under the numerical conditions given in Sec. IV, the transmission zero (in the energy interval $0 < E < 3$) cannot be found under $0 < \alpha \leqslant 83^\circ$.

[1] A. H. Castro Neto, F. Guinea, N. M. R. Peres, K. S. Novoselov, and A. K. Geim, Rev. Mod. Phys. **81**, 109 (2009).
[2] P. Dietl, F. Piéchon, and G. Montambaux, Phys. Rev. Lett. **100**, 236405 (2008).
[3] G. Montambaux, F. Piéchon, J.-N. Fuchs, and M. O. Goerbig, Phys. Rev. B **80**, 153412 (2009).
[4] P. Sinha, S. Murakami, and S. Basu, Phys. Rev. B **102**, 085416 (2020).
[5] S. Banerjee, R. R. P. Singh, V. Pardo, and W. E. Pickett, Phys. Rev. Lett. **103**, 016402 (2009).
[6] S. Banerjee and W. E. Pickett, Phys. Rev. B **86**, 075124 (2012).
[7] H. Huang, Z. Liu, H. Zhang, W. Duan, and D. Vanderbilt, Phys. Rev. B **92**, 161115(R) (2015).
[8] V. Pardo and W. E. Pickett, Phys. Rev. Lett. **102**, 166803 (2009).
[9] V. Pardo and W. E. Pickett, Phys. Rev. B **81**, 035111 (2010).
[10] Y. Hasegawa, R. Konno, H. Nakano, and M. Kohmoto, Phys. Rev. B **74**, 033413 (2006).
[11] A. S. Rodin, A. Carvalho, and A. H. Castro Neto, Phys. Rev. Lett. **112**, 176801 (2014).
[12] J. Guan, Z. Zhu, and D. Tománek, Phys. Rev. Lett. **113**, 046804 (2014).
[13] H. Duan, S. Li, S.-H. Zheng, Z. Sun, M. Yang, and R.-Q. Wang, New J. Phys. **19**, 103010 (2017).
[14] Z. J. Xiang, G. J. Ye, C. Shang, B. Lei, N. Z. Wang, K. S. Yang, D. Y. Liu, F. B. Meng, X. G. Luo, L. J. Zou, Z. Sun, Y. Zhang, and X. H. Chen, Phys. Rev. Lett. **115**, 186403 (2015).
[15] R. Fei, V. Tran, and L. Yang, Phys. Rev. B **91**, 195319 (2015).
[16] P.-L. Gong, D.-Y. Liu, K.-S. Yang, Z.-J. Xiang, X.-H. Chen, Z. Zeng, S.-Q. Shen, and L.-J. Zou, Phys. Rev. B **93**, 195434 (2016).
[17] P. Delplace and G. Montambaux, Phys. Rev. B **82**, 035438 (2010).
[18] Y. Wu, Opt. Express **22**, 1906 (2014).
[19] S. Tang and M. S. Dresselhaus, Nanoscale **4**, 7786 (2012).

[20] H. Zhang, Y. Xie, Z. Zhang, C. Zhong, Y. Li, Z. Chen, and Y. Chen, J. Phys. Chem. Lett. **8**, 1707 (2017).
[21] F. Zhai, P. Mu, and K. Chang, Phys. Rev. B **83**, 195402 (2011).
[22] Q. Li, P. Ghosh, J. D. Sau, S. Tewari, and S. D. Sarma, Phys. Rev. B **83**, 085110 (2011).
[23] C. Wang, Q. Xia, Y. Nie, M. Rahman, and G. Guo, AIP Adv. **6**, 035204 (2016).
[24] C. Zhong, Y. Chen, Y. Xie, Y.-Y. Sun, and S. Zhang, Phys. Chem. Chem. Phys. **19**, 3820 (2017).
[25] W. Meng, Y. Liu, X. Zhang, Z. He, W.-W. Yu, H. Zhang, L. Tian, and G. Liu, Phys. Rev. B **107**, 115167 (2023).
[26] A. Fakhredine, R. M. Sattigeri, G. Cuono, and C. Autieri, Phys. Rev. B **108**, 115138 (2023).
[27] J. Kim, S. S. Baik, S. H. Ryu, Y. Sohn, S. Park, B.-G. Park, J. Denlinger, Y. Yi, H. J. Choi, and K. S. Kim, Science **349**, 723 (2015).
[28] L. Tarruell, D. Greif, T. Uehlinger, G. Jotzu, and T. Esslinger, Nature (London) **483**, 302 (2012).
[29] B. Real, O. Jamadi, M. Milićević, N. Pernet, P. St-Jean, T. Ozawa, G. Montambaux, I. Sagnes, A. Lemaître, L. Le Gratiet, A. Harouri, S. Ravets, J. Bloch, and A. Amo, Phys. Rev. Lett. **125**, 186601 (2020).
[30] P. Sinha, S. Murakami, and S. Basu, Phys. Rev. B **105**, 205407 (2022).
[31] F. Zhai and J. Wang, J. Appl. Phys. **116**, 063704 (2014).
[32] W. J. Chan, L. Ang, and Y. S. Ang, Appl. Phys. Lett. **122**, 163102 (2023).
[33] W. Chen, X. Zhu, X. Zhou, and G. Zhou, Phys. Rev. B **103**, 125429 (2021).
[34] S. Rostamzadeh and M. Sarisaman, New J. Phys. **24**, 083026 (2022).
[35] H. Li, X. Hu, and G. Ouyang, New J. Phys. **24**, 053049 (2022).
[36] H.-J. Duan, Y.-J. Wu, Y.-Y. Yang, S.-H. Zheng, C.-Y. Zhu, M.-X. Deng, M. Yang, and R.-Q. Wang, New J. Phys. **24**, 033029 (2022).
[37] F. Goos and H. Hänchen, Ann. Phys. **436**, 333 (1947).
[38] D. Felbacq and R. Smaâli, Phys. Rev. Lett. **92**, 193902 (2004).
[39] F. Wu, J. Wu, Z. Guo, H. Jiang, Y. Sun, Y. Li, J. Ren, and H. Chen, Phys. Rev. Appl. **12**, 014028 (2019).
[40] F. Wu, M. Luo, J. Wu, C. Fan, X. Qi, Y. Jian, D. Liu, S. Xiao, G. Chen, H. Jiang, Y. Sun, and H. Chen, Phys. Rev. A **104**, 023518 (2021).
[41] X. Chen, X.-J. Lu, Y. Ban, and C.-F. Li, J. Opt. **15**, 033001 (2013).
[42] Z.-M. Yu, Y. Liu, and S. A. Yang, Front. Phys. **14**, 33402 (2019).
[43] X. Ling, Z. Zhang, S. Chen, X. Zhou, and H. Luo, J. Phys. D **55**, 133001 (2022).
[44] Z.-Y. Wang, Z.-X. Li, H.-Y. Yuan, Z.-Z. Zhang, Y.-S. Cao, and P. Yan, Acta Phys. Sin. **72**, 057503 (2023).
[45] Z. Wu, F. Zhai, F. M. Peeters, H. Q. Xu, and K. Chang, Phys. Rev. Lett. **106**, 176802 (2011).
[46] F. Zhai, Y. Ma, and K. Chang, New J. Phys. **13**, 083029 (2011).
[47] Y. Song, H.-C. Wu, and Y. Guo, Appl. Phys. Lett. **100**, 253116 (2012).
[48] X. Zhou, J. Zheng, and F. Zhai, Commun. Theor. Phys. **74**, 075701 (2022).
[49] C. Zhang, J. Yang, S.-H. Zhang, and W. Yang, J. Appl. Phys. **132**, 184302 (2022).
[50] A. Huamán and G. Usaj, Phys. Rev. A **100**, 033409 (2019).
[51] H. Ghadiri and A. Saffarzadeh, Phys. Rev. B **105**, 085415 (2022).
[52] Y. Liu, Z.-M. Yu, H. Jiang, and S. A. Yang, Phys. Rev. B **98**, 075151 (2018).
[53] Q.-D. Jiang, H. Jiang, H. Liu, Q.-F. Sun, and X. C. Xie, Phys. Rev. Lett. **115**, 156602 (2015).
[54] N. K. Dongre and K. Roychowdhury, Phys. Rev. B **106**, 075414 (2022).
[55] U. Chattopadhyay, L. K. Shi, B. Zhang, J. C. W. Song, and Y. D. Chong, Phys. Rev. Lett. **122**, 066602 (2019).
[56] M. Yang, Q.-T. Hou, and R.-Q. Wang, New J. Phys. **22**, 033015 (2020).
[57] W. Porod, Z. A. Shao, and C. S. Lent, Appl. Phys. Lett. **61**, 1350 (1992).
[58] Z. A. Shao, W. Porod, and C. S. Lent, Phys. Rev. B **49**, 7453 (1994).
[59] I. Rotter and A. F. Sadreev, Phys. Rev. E **71**, 046204 (2005).
[60] F. Zhai and H. Q. Xu, Phys. Rev. B **72**, 195346 (2005).
[61] D. Kang, W. Ju, S. Zhang, and C. Xia, Phys. Chem. Chem. Phys. **21**, 25993 (2019).
[62] S. S. Baik, K. S. Kim, Y. Yi, and H. J. Choi, Nano Lett. **15**, 7788 (2015).
[63] J. Jang, S. Ahn, and H. Min, 2D Mater. **6**, 025029 (2019).
[64] C. W. J. Beenakker, R. A. Sepkhanov, A. R. Akhmerov, and J. Tworzydło, Phys. Rev. Lett. **102**, 146804 (2009).
[65] L. Zhao and S. F. Yelin, Phys. Rev. B **81**, 115441 (2010).
[66] T. Ando, Phys. Rev. B **44**, 8017 (1991).
[67] H. Xu, Phys. Rev. B **50**, 8469 (1994).
[68] F. Zhai and J. Lu, Phys. Rev. B **94**, 165426 (2016).